Potential of GNSS-R for the Monitoring of Lake Ice Phenology

Yusof Ghiasi, *Student Member, IEEE*, Claude R. Duguay, *Member, IEEE*, Justin Murfitt, Milad Asgarimehr, *Member, IEEE*, and Yuhao Wu

***Abstract*—This article introduces the first use of global navigation satellite system (GNSS) reflectometry for monitoring lake ice phenology. This is demonstrated using Qinghai Lake, Tibetan Plateau, as a case study. Signal-to-noise ratio (SNR) values obtained from the cyclone GNSS (CYGNSS) constellation over four ice seasons (2018 to 2022) were used to examine the impact of lake surface conditions on reflected GNSS signals during open water and ice cover seasons. A moving *t*-test algorithm was applied to time-varying SNR values allowing for the detection of lake ice at daily temporal resolution. Good agreement was achieved between ice phenology records derived from CYGNSS data and Moderate Resolution Imaging Spectroradiometer (MODIS) imagery. The CYGNSS timings for freeze-up, i.e., the period starting with the first appearance of ice on the lake (freeze-up start; FUS) until the lake becomes fully ice covered (freeze-up end; FUE), as well as those for breakup, i.e., the period beginning with the first pixel of open water (breakup start; BUS) and ending when the whole lake becomes ice-free (breakup end; BUE), were validated against the phenology dates derived from MODIS images. Mean absolute errors are 7, 5, 10, 4, and 5 days for FUS, FUE, BUS, BUE, and ice cover duration, respectively. Observations revealed the sensitivity of GNSS reflected signals to surface melt prior to the appearance of open water conditions as determined from MODIS, which explains the larger difference of 10 days for BUS.**

***Index Terms*—Cyclone GNSS (CYGNSS), global positioning satellite system reflectometry (GNSS-R), lake ice, phenology, Qinghai Lake.**

Manuscript received 25 July 2023; revised 4 October 2023; accepted 30 October 2023. Date of publication 7 November 2023; date of current version 29 November 2023. This work was supported in part by the Transformative Sensor Technologies and Smart Watersheds project under the Global Water Futures Program with funding from the Canada First Research Excellence Fund, and in part by the Natural Sciences and Engineering Research Council of Canada under Grant RGPIN-2017-05049 to Claude Duguay. *(Corresponding author: Yusof Ghiasi.)*

Yusof Ghiasi is with the Department of Geography and Environmental Management, University of Waterloo, Waterloo, ON N2L 3G1, Canada (e-mail: syghiasi@uwaterloo.ca).

Claude R. Duguay is with the Department of Geography and Environmental Management, University of Waterloo, Waterloo, ON N2L 3G1, Canada, and also with the H2O Geomatics Inc., Kitchener, ON N2G 1H6, Canada (e-mail: crduguy@uwaterloo.ca).

Justin Murfitt and Yuhao Wu are with the H2O Geomatics Inc., Kitchener, ON N2G 1H6, Canada (e-mail: jmurfitt@uwaterloo.ca; y494wu@uwaterloo.ca).

Milad Asgarimehr is with the Institute of Geodesy and Geoinformation Science, Technische Universität Berlin, 10623 Berlin, Germany, also with the Signal Theory and Communications Department, Universitat Politecnica de Catalunya, 08034 Barcelona, Spain, and also with the German Research Centre for Geosciences, 14473 Potsdam, Germany (e-mail: milad.asgarimehr@gfz-potsdam.de).

Digital Object Identifier 10.1109/JSTARS.2023.3330745

I. Introduction

THE seasonal cycle and duration of lake ice cover (LIC), which involves the time between freeze-up and breakup periods, are described by ice phenology [1]. Freeze-up covers the period between freeze onset (the first appearance of ice) and when a complete ice sheet covers the lake surface, often referred to as freeze-up start (FUS) and freeze-up end (FUE), respectively. Similarly, breakup corresponds to the period between the first appearance of open water and full disappearance of ice from the lake surface [1], also commonly known as breakup start (BUS) and breakup end (BUE), respectively. The presence/absence and extent of ice cover and ice thickness as well as freezing duration (FD) and breaking duration (BD) during winter months have wide-ranging impacts on lake–atmosphere interactions, e.g., lake-effect snowfall, thermal moderation (e.g., [3], [4]), aquatic ecosystems [5], and human activities ranging from winter transportation and hydroelectric power generation to ice skating and religious ceremonies [6]. LIC and thickness have been noted as sensitive indicators of climate change and, as such, are identified as thematic products of lakes as an essential climate variable by the Global Climate Observation System [7], [8]. Recent long-term trends in lake ice phenology for northern lakes show an average shortening of ∼17 days in the duration of ice over the last century [9]. Analyzing lake ice phenology records from 1855 to 2019, Sharma et al. [9] found that freeze-up has been occurring, on average, ∼11 days later, while breakup has been starting ∼7 days earlier per century. While ground-based observational sites have provided much of the evidence for changes in ice phenology (e.g., [10]), the number of sites has dwindled in the last 40 years [11], [12]. In this respect, satellite remote sensing is playing an increasingly important role in monitoring lake ice phenology and documenting recent changes [11], [13], [14], [15].

Satellite remote sensing of LIC is either based on the use of optical, passive microwave, or active microwave data, each presenting some advantages and limitations [12]. Among the data sources, those from optical remote sensing satellite missions are available with extended time series [ca. 20 years for Moderate Resolution Imaging Spectroradiometer (MODIS) and ca. 40 years for Landsat] and at varying resolutions (ca. 30 m for Landsat and ca. 500 m for MODIS); however, the quality of the ice phenology records from these data is impacted by the presence of cloud cover and low solar illumination conditions/darkness. Passive microwave instruments are not influenced by the latter but, due to the low spatial resolution they provide (tens of km

footprints, interpolated onto ca. 3–10 km grids), ice phenology can be retrieved from very large lakes only [15], [16], [17]. While active microwave sensors, such as synthetic aperture radar, can also operate under all-weather and light conditions, and are increasingly providing better historical records at relatively high temporal resolution for high-latitude lakes (e.g., 1–2 days for Sentinel-1 [18]), their instrumentations tend to be costly for finer temporal and spatial resolutions due to complicated board designs and high-power demands [19]. Meanwhile, global navigation satellite system reflectometry (GNSS-R), as an active–passive microwave tool, is a novel remote sensing technique at a low cost that provides high temporal and spatial resolutions for a variety of ocean and land applications [20]. GNSS-R is a remote sensing technique based on receiving and processing reflected navigational L-band signals from sea and land. Hall and Cordy [21] proposed the use of reflected GNSS signals as a bistatic radar technique for the first time, which was later followed by Martín-Neira [22] who presented the idea of ocean altimetry using GNSS-R.

GNSS-R has been proposed and used for various applications in cryosphere remote sensing as part of ground-based, aerial, and spaceborne platforms. The use of GNSS-R for ice remote sensing was first demonstrated by [23] with an airborne receiver for sea ice detection. Proceeding this experiment, several ground-based GNSS-R experiments for ice remote sensing have been conducted. Among them, [24] and [25], and later, [26] accomplished ground-based experiments to study sea ice concentration by analyzing signal polarization ratios. Ground-based GNSS-R is among the multiple sensors that were deployed during the multidisciplinary drifting observatory for the study of Arctic climate expedition to monitor sea ice properties [27]. Jacobson [28] and [29] proposed the potential of GNSS-R for estimating lake ice thickness (LIT), a concept that was further explored by [30] at sub-Arctic lake ice sites and achieved average errors of 0.07 m in LIT retrievals when compared to manual measurements (drilled holes with auger in the ice). Several space-based GNSS-R experiments have also been carried out for sea ice detection using data acquired by the U.K.-DMC and TDS-1 satellites. Moreover, two recent spaceborne GNSS-R missions, namely Spire and Federated Satellite Systems/3Cat, have shown potential for sea ice characterization, including ice concentration and ice type as well as sea surface height [31], [32], [33].

Few studies have explored signals recorded by spaceborne GNSS-R systems to detect or monitor lake ice properties. One GNSS-R spaceborne platform with potential for lake ice monitoring is the cyclone GNSS (CYGNSS) constellation system. It is the first GNSS-R pathfinder mission consisting of eight low Earth orbiting microsatellites. CYGNSS was launched in December 2016 with the main objective of monitoring near-surface ocean wind and currents monitoring (e.g., [34], [35], [36]); however, it can also be used as a remote sensing tool for remote sensing of other environmental characteristics, including, but not limited to, inland water monitoring (e.g., [37], [38], [39]), soil moisture, wetlands, and biomass observation [41], [42], [43], freeze/thaw state retrieval [44], [45], and mesoscale ocean eddies observations [46]. Mayer and Ruf [47] proposed the potential of CYGNSS for conducting altimetry over lake ice and using the transparency of ice to GNSS L-band signals to infer ice thickness. Li et al. [48] found the first evidence of freshwater ice effects on CYGNSS altimetry over Qinghai Lake, Tibetan Plateau, during winter 2018, by observing a lower water level during the ice season. Recently, Zavorotny et al. [49] used CYGNSS raw data collected from three specular tracks over Qinghai Lake to investigate the scattering coherency of the lake in both open water and frozen states. The latter research suggested higher variability in the signal-to-noise ratio (SNR) reflected from the ice compared to that of open water due to the lower Fresnel reflection coefficient of the ice layer compared to the surface water. In addition, the authors considered the interference between signals reflected from the top and the bottom of the ice, as well as changes in surface roughness and ice thickness within a specular track as other parameters leading to the larger SNR fluctuation.

The primary objective of this article was to develop and evaluate an approach for the determination of lake ice phenology through the application of changes in CYGNSS SNR values. To this end, SNR values from CYGNSS level-1 data were extracted over Qinghai Lake (Tibetan Plateau, China) from August 2018 to August 2022, encompassing four ice seasons.

The rest of this article is organized as follows. The study area is briefly introduced in Section II. The main dataset along with auxiliary data, as well as the methodology are explained in Section III. Results and discussion are presented in Sections IV and V, respectively. Finally, Section VI concludes this article.

II. Study Area

The largest lake that forms a complete ice cover within the area covered by CYGNSS (±38° in latitudes) is Qinghai Lake (Fig. 1). The lake is located in the northeast part of the Tibetan Plateau (Lat: 36°32′ to 37°15′N, Lon: 99°36′ to 100°47′E) at an altitude of 3260 m above sea level. Qinghai Lake is among the most noticeable lakes on the Tibetan Plateau and has been a lake of interest in several previous investigations, including, but not limited to, lake ice phenology, animal species living in the area, and tourism [50]. Therefore, the lake was chosen as the best candidate to examine the capability of CYGNSS to monitor lake ice phenology.

Qinghai Lake has a convex shape with a tortuous coastline and contains two small islands. The lake is the largest inland waterbody of the Tibetan Plateau, filled with weakly saline–alkaline water (salinity = 15.18 g/l; pH = 9.2) [51]. The average area of Qinghai is 4300 km^2 with an average depth of 18.3 m and maximum of 26.6 m. The annual average temperature is 0.5°C [51]. In Qinghai Lake, the freeze-up period usually begins in mid-December and lasts until early January. The breakup period starts during the second half of March and ends in early April [52].

III. Data and Methods

A. CYGNSS Data

The main data product of CYGNSS are delay-Doppler maps (DDMs), which are the cross-correlation power of the forward scattered signal with its replica generated locally at the receiver,

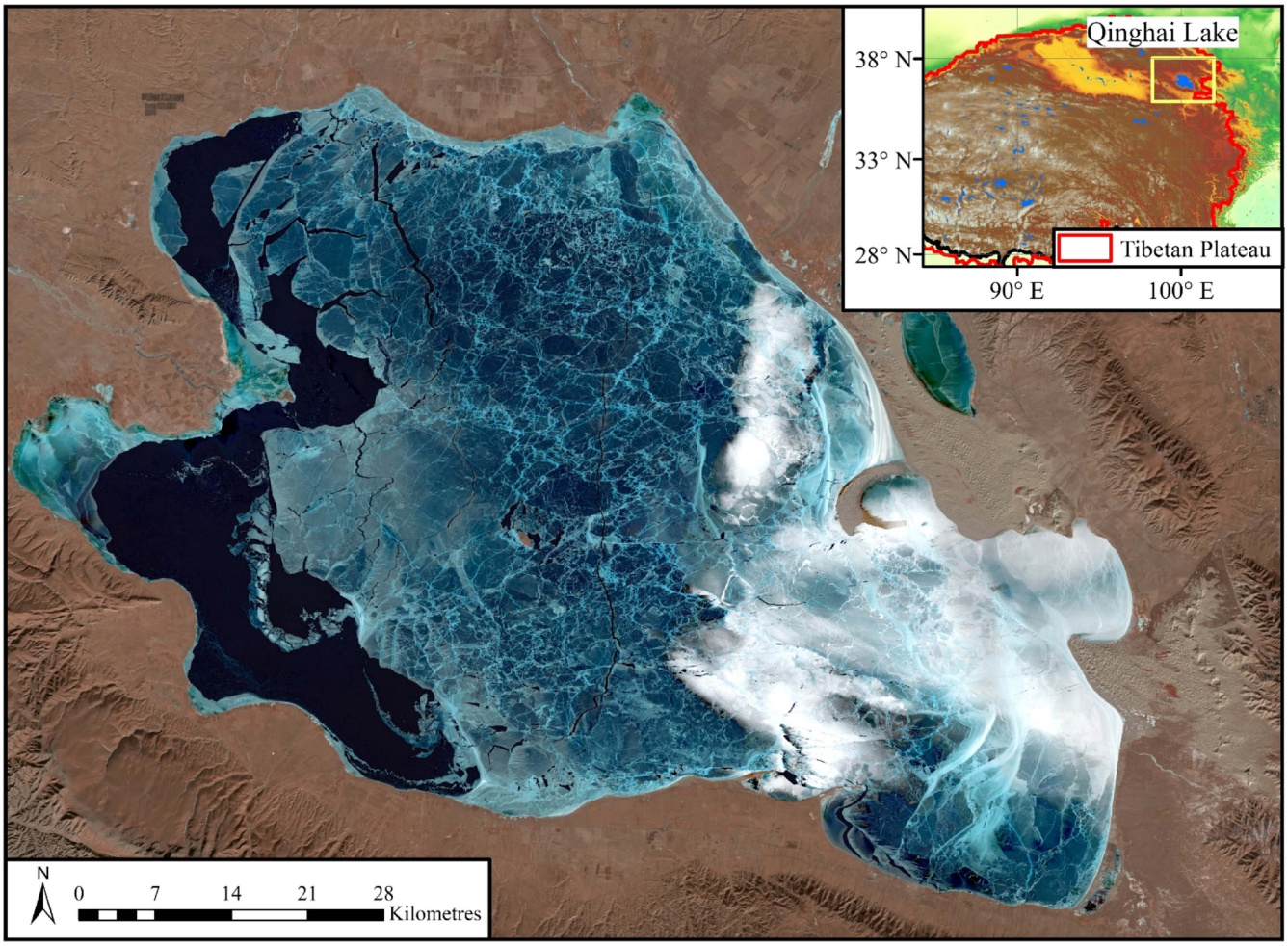

Fig. 1. Location of Qinghai Lake on the Tibetan Plateau. Landsat-8 level-1 OLI/TIRS image courtesy of the United States Geological Survey (USGS) Digital Object Identifier (DOI) number: /10.5066/F71835S6. Topographic is also courtesy of the USGS, GTOPO30 Hydro1K, DOI number: /10.5066/F77P8WN0.

in a range of delay and Doppler frequency shifts. Radar observables can be extracted from the DDMs and are stored as metadata in the CYGNSS level-1 data products. The data are available to users in netCDF format through the Physical Oceanography Distributed Active Archive Center database. More details on CYGNSS data products are provided in [53]. This article used CYGNSS level-1 version 3.0 data covering the period from 1 August 2018 to 1 August 2022, which encompass four full ice seasons. The key observations used in this article are the SNR values of the DDMs, which have already been calculated and included among the CYGNSS metadata. Due to the high temporal revisit of the CYGNSS constellation, with an average revisit time of 7 h, 117 190 specular points were obtained from 7140 specular tracks. Over the four ice seasons of this article, the average number of footprints per day was 62 (maximum 260 and minimum 1), which were collected through, on average, two daily specular tracks over the lake. The average SNR values were then calculated with an average variance of 0.05 for each day. Average daily SNR values were used to analyze the impact of surface conditions on SNR and determine ice phenology.

Low SNR measurements are frequently encountered on land, which can be attributed to either the specular point's position within the CYGNSS antenna pattern or a minimal amount of surface scattering [54]. Consequently, it is crucial to exclude measurements with low SNR from the time-series retrieval process because they exhibit inferior measurement quality. Therefore, observations with SNR values below zero are also excluded.

B. Moderate Resolution Imaging Spectroradiometer (MODIS) Images

MODIS true color composite (Red = band 1, Green = band 4, and Blue = band 3; [55]) images were used to visually determine dates associated with the freeze-up and breakup periods, which were compared to the dates obtained from CYGNSS. In MODIS RGB images, the freeze-up period was identified as the first date where the ice cover was visible (FUS) until the first date when the ice cover fully covered the lake surface (FUE). The breakup period was identified as the period between the date of the first appearance of water (BUS) and the full disappearance of the ice cover from the lake (BUE). Next, the difference between FUS, FUE, BUS, and BUE dates determined from MODIS and CYGNSS was compared by calculating the mean bias error (MBE) and the mean absolute error (MAE). Ice cover duration

(ICD), which is the date from the FUE to the BUE periods, as well as FD and BD, were also calculated. It is worth noting that the reliability of MODIS images is influenced by the presence of clouds, and this introduces some uncertainty in the precise visual determination of the phenology dates. Considering the utilization of both Terra and Aqua images, the average frequency of cloud cover in MODIS images during FUS, FUE, BUS, and BUE periods were two days over Qinghai Lake, which caused two days uncertainty in the determination of timing of ice phenology.

C. MODIS Derived Products

In addition to MODIS color composite images, three MODIS-derived geophysical products were obtained to provide further evidence of the sensitivity of CYGNSS SNR values to lake surface conditions and to determine ice phenology. Land surface temperature (LST; MOD/MYD11A1, daily, level 3, version 6) and surface albedo (MOD/MYD10A1, daily, level 3, version 6), which are both also retrieved over inland waterbodies, were downloaded from the NASA Land Processes Distributed Active Archive Center. LST and surface albedo have been found to be useful complements in the interpretation of changes in lake surface conditions during the freeze-up and breakup periods, and the development of an ice phenology retrieval algorithm from spaceborne scatterometer observations [56].

LST data were processed by averaging day and night observations from both Terra and Aqua over the entire lake for each day. According to previous validation efforts conducted by [57] and [58], MODIS LST products have shown a bias of less than 1 K compared to in-situ measurements with a mean difference of 0.27 K against ground-based LST data obtained over the Tibet Plateau [59]. MODIS LST have been shown to be a reliable data source for quantifying climate variability, monitoring lake surface water temperature, and detecting lake ice over Tibetan Lakes [60], [61]. Daily LST data were used in support of the interpretation of seasonal drops and increases in SNR values with freeze-up and break-up (Sections IV-A and IV-B).

MODIS daily albedo products were used in concert with minimum, mean, and maximum surface temperatures derived from ERA5-Land hourly data (Section III-D) to detect the beginning of snow/ice surface melt before the first appearance of open water (i.e., BUS). The albedo products are generated only for clear-sky dates and snow-covered surfaces [62], which characterize the reflectance anisotropy of MODIS pixels at the spatial resolution of 500 m [63], [64]. These data have previously been used to analyze the breakup period [65], [66]. In this article, the average albedo for the whole lake was calculated for each day and used to determine the dates of beginning of surface melt, which are marked by a general continuous decrease in albedo until the appearance of open water (BUE). Since clear-sky conditions are not encountered on each day, the surface albedo values were compared with MODIS images and found to provide, on average, an uncertainty of one day during the melt onset period for the four ice seasons of analysis.

The third product used is the Lakes_cci dataset (version 2.02) produced as part of the climate change initiative of the European Space Agency (ESA). It is a daily product on a common harmonized grid (at 1/120° or ca.1-km latitude–longitude) consisting of five thematic variables, including lake water level, lake water extent, lake surface water temperature, LIC, and lake water-leaving reflectance [67], [68]. Among them, this article used the LIC thematic variable, which is mapped at the global scale based on a random forest classifier using Terra/Aqua MODIS top-of-atmosphere reflectance data [14]. Here, the LIC dataset is used as a complementary source for comparison of CYGNSS SNR values against the lake surface conditions (ice/water) and evaluate the sensitivity of CYGNSS to lake ice. In the LIC dataset, each lake pixel is classified as either water (=1), ice (=2), cloud (=3), and bad/unusable data (=4). Here, we excluded those pixels flagged as 3 and 4, and only used the ones classified as water or ice. The overall classification accuracy of this data product, which uses a combination of seven bands, has been reported to be greater than 97% [67]. However, product uncertainty increases during breakup and freeze-up periods, where the mixture of ice and water increases the confusion in the classification process. To mitigate this issue, we applied a seven-day moving average to examine the sensitivity of CYGNSS SNR values to the presence of lake ice or open water. The Lakes_cci data product (version 2.02) covers up to the end of 2020. However, a third ice season that encompasses the breakup period of 2021 was added to the LIC dataset since some coauthors of this article are also contributors to ESA Lakes_cci product. Year 2022 will only be added in a future release of the product such that three of four ice seasons could be compared with SNR values.

D. ERA5-Land Lake Ice Surface Temperature

To calculate daily minimum, mean, and maximum temperatures of the lake ice surface, we obtained hourly ERA5-Land reanalysis data from the European Centre for Medium Range Weather Forecasts, which comprises a variety of lake related variables including temperature of the uppermost ice surface [69]. The spatial resolution of the ERA5-Land dataset is 9 km. Daily minimum, mean, and maximum lake ice surface temperatures slightly prior to and during the melt period were used, along with MODIS albedo data, to estimate the melt onset dates. The decrease in surface albedo is highly dependent on the melt of lake ice in spring, which is strongly controlled by surface temperature (melting versus subfreezing) [1].

E. Determination of Ice Phenology From GNSS-R

In spaceborne GNSS-R, the primary scattering mode of interest is coherent reflection, in which the GNSS signals are reflected from extremely smooth surfaces compared to the wavelength, where mirror-like reflection is expected. In CYGNSS, in the case of coherent reflection, the glistening zone is approximately 0.5 to 1 km for a single pixel in DDM causing a constructive interference between scattered signals [70], [71]. For inland targets, both coherent and incoherent reflection/scattering can dominate CYGNSS observations due to their properties, such as topography and small-scale roughness [72]. On frozen lakes, the multilayer scattering regime is another potential source for the extinction of coherent reflection, which will be discussed

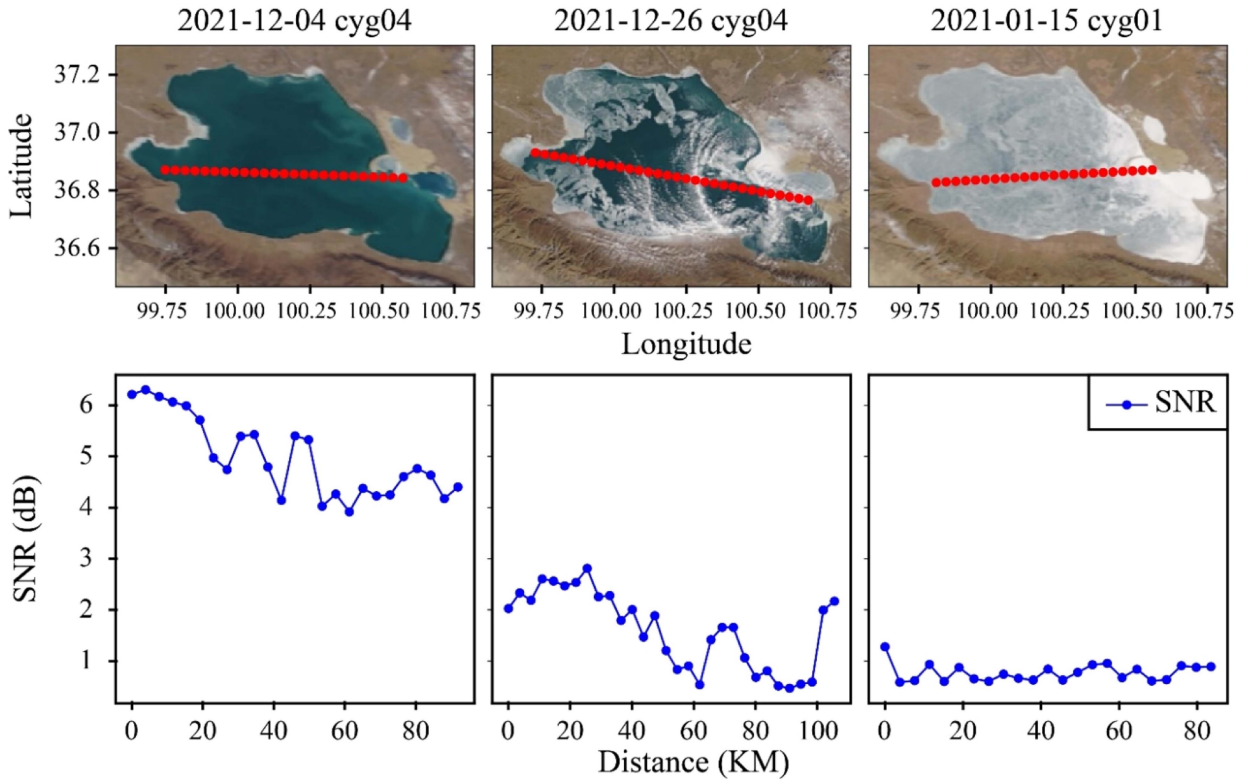

Fig. 2. (Top) CYGNSS tracks over Qinghai Lake under three conditions: Open water (left), mix of ice and water during the freeze-up period (center), and fully ice covered (right) during the 2021–2022 ice season. (Bottom) Variations in SNR along each track. The annotation cyg0# in each subplot indicates which CYGNSS satellite was used for the observation. Images courtesy: MODIS-aqua.

in the next section. Several approaches have been suggested in previous articles to examine coherent reflection, including, but not limited to, the assessment of DDM SNR [73], [74], DDM trailing edge slope [75], [76], and DDM power spread extent [71]. In this article, we only examined the DDM SNR values to analyze the reflectivity of Qinghai Lake.

It is pertinent to note that alternative observables beyond SNR could be used in this article, including reflectivity and the normalized bistatic radar cross-section (NBRCS). These parameters have been employed in prior research for soil moisture retrievals. However, our investigation in this article was only focused on SNR for two principle reasons. First, NBRCS calculations were not conducted for all inland specular points due to the absence of effective scattering area data in CYGNSS metadata files. Second, reflectivity, another viable parameter, exhibited notably similar patterns in our region of study; therefore, we opted to exclusively examine SNR as it does not require additional calculations as does reflectivity [77].

To determine lake ice phenology, a moving *t*-test (MTT) was employed to detect abrupt changes in the CYGNSS SNR time series by calculating the difference between the mean values of two subsamples. The MTT method, which was initially developed for abrupt change detection in climate data [78], [79], has shown a strong ability in lake ice detection from satellite passive microwave data [15], [16]. The temporal subsample size was chosen as 30 days to exclude possible short-term SNR changes. In other words, the 30-day subsamples were first selected, by moving, from the time series of daily SNR observations, and the *t*-scores were then calculated for each two consecutive subsamples, as suggested by [16] as follows:

$$t = \frac{\overline{x_{k2}} - \overline{x_{k1}}}{S_k \sqrt{\frac{1}{n_1} + \frac{1}{n_2}}} \tag{1}$$

where $\overline{x_{k1}}$ and $\overline{x_{k2}}$ are the mean values of each consecutive subsample, n_1 and n_2 are the size of subsamples (=30 days), and S_k is the variance factor calculated based on the variances for two subsamples (S_{k1}^2 and S_{k1}^2) as follows:

$$S_k = \sqrt{\frac{n_1 S_{k1}^2 + n_2 S_{k2}^2}{n_1 + n_2 - 2}}. \tag{2}$$

Then, under the confidence level of 0.001, periods with $|t| > t_{0.001}$ were determined as dates in which abrupt changes happened. When an abrupt change is detected and the *t*-statistic is positive, it is considered part of the breakup period; however, if the *t*-statistic is negative, then it is part of the freeze-up period.

IV. Results

A. Impact of Lake Surface Conditions on SNR Values

Figs. 2 and 3 present a set of examples of CYGNSS tracks along with DDM SNR variations under different lake surface conditions (open water, mix of ice and water, and fully ice-covered) during the freeze-up and breakup periods of ice season 2021–2022. Fig. 2 reveals a decrease in SNR

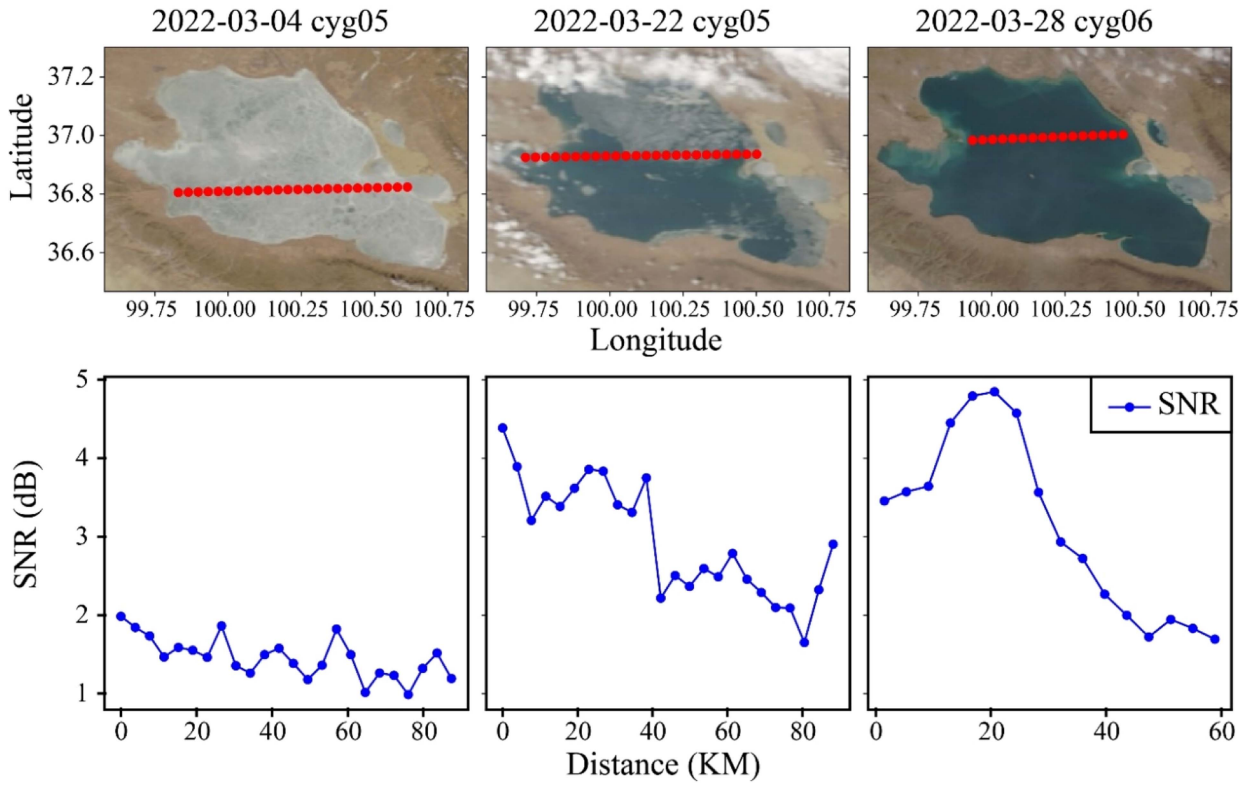

Fig. 3. (Top) CYGNSS tracks over Qinghai Lake under three conditions: fully ice covered before breakup start (left), mix of ice and water during the breakup period (center), and open water (right) during the 2021–2022 ice season. (Bottom) Variations in SNR along each track. The annotation cyg0# in each subplot indicates which CYGNSS satellite was used for the observation. Images courtesy: MODIS-Aqua.

values as the lake transitions from open water to partially and then fully ice-covered conditions. Similarly, Fig. 3 shows the sensitivity of SNR values to changing lake surface conditions just before and during the breakup period in spring 2022.

Fig. 4 shows the impact of lake surface conditions during open water and ice cover seasons on reflected GNSS signals (aggregated lake-wide) over the 4-year ice seasons. SNR fluctuations of the reflected GNSS signals from the lake indicate a lower reflection from ice cover and, in contrast, a higher reflection from open water. This is expected to be due to the low salinity of lake ice (12 ppt for Qinghai Lake), which results in a lower loss factor for L-band signals than, for example, first-year sea ice [80]. The thickening of ice on the lake causes an interference between signals reflected from the ice surface and the ice–water interface; therefore, the single-scattering regime assumption suggested by [20] may not be preserved, which results in significant variations in SNR values during the ice season as discussed in [49] and seen in Fig. 4. Our observations during the 4-year study period show that the average of CYGNSS SNR values during the ice growth period remains below 1.66 dB with standard deviation of 0.84, while it increases to 3.1 dB (standard deviation = 1.4) when the lake condition is open water.

Furthermore, when Lakes_cci LIC data are compared with CYGNSS SNR values, there is a strong relationship between the presence of ice cover and low SNR values. Fig. 5 displays a seven-day moving average applied to the Lakes_cci LIC data (1 = water; 2 = ice) along with that of CYGNSS SNR values from the whole surface of the lake. When comparing these two datasets, 86% of pixels classified as ice by Lakes_cci LIC (class 2) have SNR values below 1.66 dB, which is the average value of CYGNSS SNR recorded during the freeze-up period. On the other hand, 82% of the SNR observations with values below 1.66 dB are from areas that are flagged as lake ice in the Lakes_cci LIC data product.

B. Lake Ice Phenology Determination From SNR Values

Fig. 6 shows the SNR time series, the t-scores obtained from the MTT method, and the phenology dates determined using MODIS RGB color composite images and CYGNSS SNR analysis. In addition, Table I contains the dates associated with ice phenology and ICD derived from CYGNSS and those determined from the interpretation of MODIS RGB images from August 2018 to August 2022. Results show a generally good agreement between visually determined freeze-up and breakup periods and those dates that correspond to abrupt changes in CYGNSS SNRs detected from the MTT method [i.e., t-scores calculated from (1) and (2)]. Furthermore, the maximum absolute t-score values (MTT spike in Table I) occur within the freeze-up and breakup periods visually obtained from MODIS images. This demonstrates the ability of GNSS signals to determine lake ice phenology events.

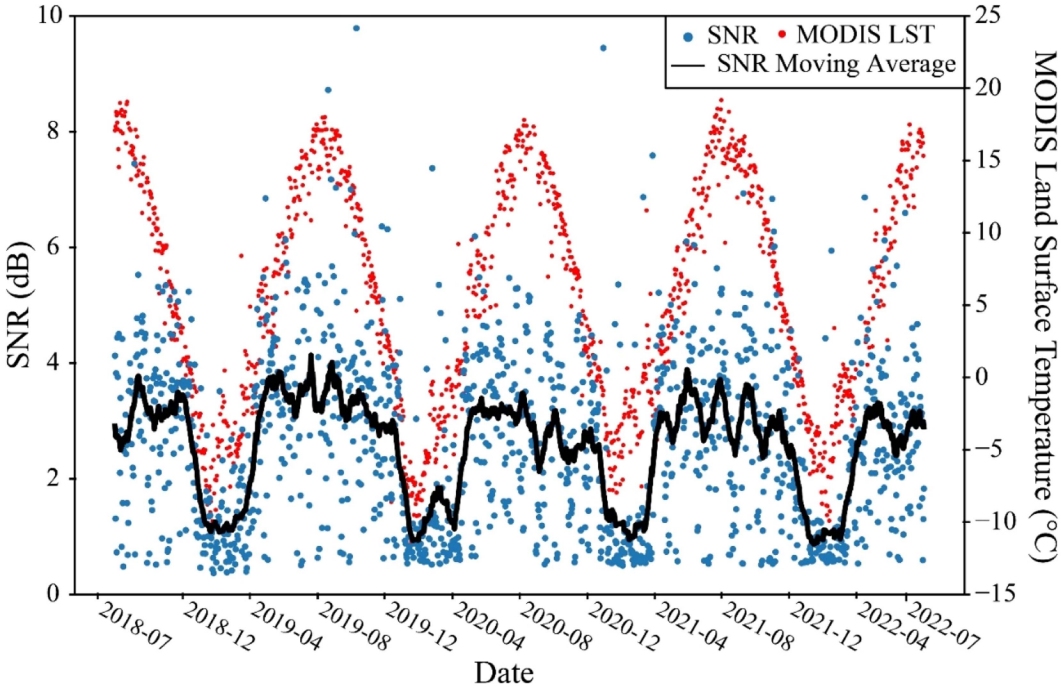

Fig. 4. Variations in CYGNSS SNR (aggregated lake-wide) values over Qinghai Lake (light blue) with a 30-day moving average (dark blue) showing lower reflections during wintertime. MODIS LST variations are shown in dark/light red.

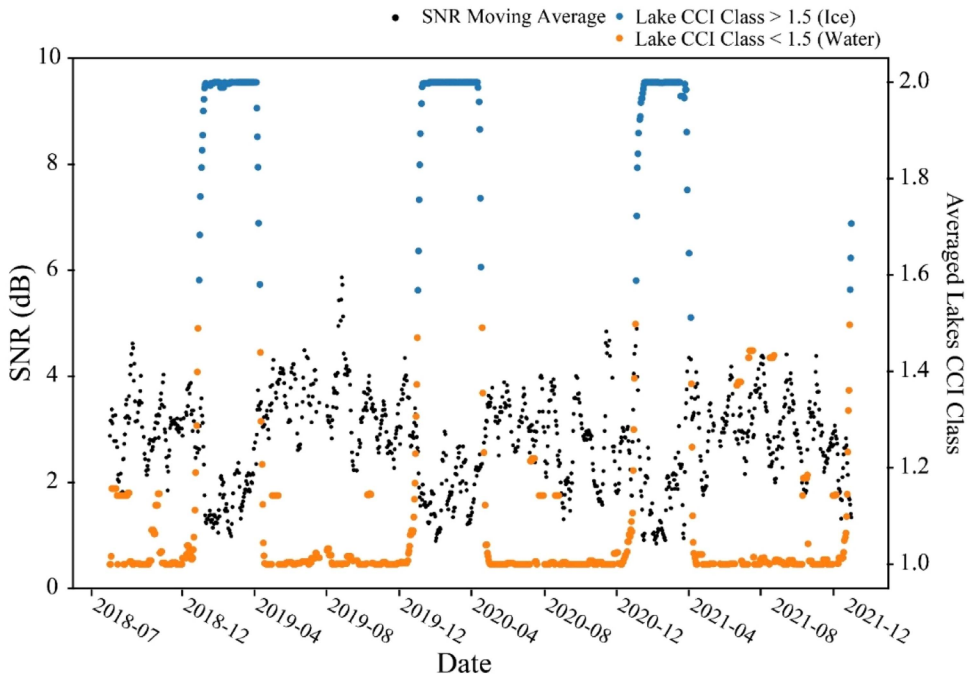

Fig. 5. CYGNSS SNR values (blue dots) and Lakes_cci LIC classification from a 7-day moving average. Orange dots correspond to when the moving average for the LIC classification was less than 1.5 (water) and blue dots correspond to when the moving average for the LIC classification was greater than 1.5 (ice). Points where the average is greater than 1.5 likely correspond to the ice season, which matches well the drops in CYGNSS SNR values.

V. Discussion

A. Lake Ice Impact on GNSS-R Coherence

Depending on the surface roughness, the GNSS signal reflection is composed of two coherent and incoherent components. The surface roughness weakens the reflection coherency and is inversely correlated with the power. At first glance, it might be intuitively assumed that ice over the lake surface can prevent formation of waves, and therefore, due to the roughness decrease, the coherent reflection is intensified. This is a common case seen over sea, as the sea ice results in higher reflection power than sea water. However, this assumption ignores the role of the Fresnel

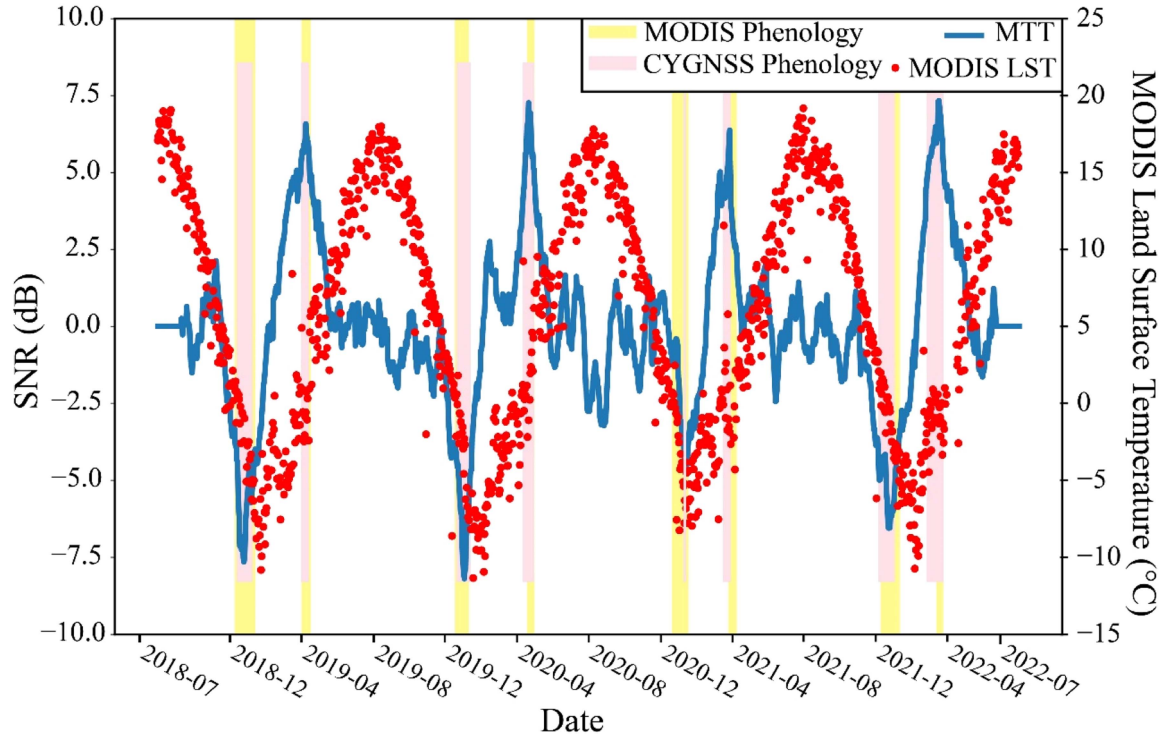

Fig. 6. CYGNSS SNR MTT from 1 August 2018 to 1 August 2022. Pink bars are ice phenology periods obtained from CYGNSS and yellow bars are those visually determined from MODIS images over four FU and four BU periods. MODIS LST values are also plotted (brown dots) to show that the timing of the FU and BU periods closely match below and above freezing temperature of 0°C, respectively.

TABLE I
SUMMARY OF FU AND BU PERIODS, ICD, AND MTT SPIKE DATES FOR EACH YEAR FROM 2018 TO 2022 DETERMINED FROM CYGNSS DATA AND MODIS IMAGES

	2018-2019		2019-2020		2020-2021		2021-2022	
	FU	BU	FU	BU	FU	BU	FU	BU
MODIS	Dec 9 – Jan 13	Apr 4 – Apr 18	Dec 18 - Jan 11	Apr 18 – May 1	Dec 20 - Jan 17	Mar 26 - Apr 9	Dec 10 - Jan 11	Mar 16 – Mar 25
CYGNSS	Dec 13 – Jan 9	Apr 1 – Apr 14	Dec 21 - Jan 14	Apr 10 - Apr 30	Jan 10 - Jan 12	Mar 17 -Mar 29	Dec 6- Jan 2	Feb 26 – Mar 26
MTT spike	Dec 25	Apr 9	Jan 4	Apr 24	Jan 10	Mar 28	Dec 27	Mar 19
MODIS ICD	95 days		110 days		82 days		73 days	
CYGNSS ICD	95 days		106 days		76 days		83 days	

reflection coefficient, which in turn is controlled by the surface permittivity. The permittivity is also dependent on the salinity, which therefore suggests different behaviors over sea and lakes. In addition, over ice, unlike liquid water, a multilayer reflection can apply, which will lead to a decrease in the reflection power due to the interference between signals reflected from the top and bottom of the ice and by different layers. As a result, the drop in SNR over lake ice is physically plausible, and such behavior has also been documented in other lake ice studies using GNSS-R [49].

According to [81], three attenuation factors can be considered for the DDM power obtained from inland targets, which are the power Fresnel reflection coefficient driven by the dielectric properties of the surface, the decorrelation factor controlled

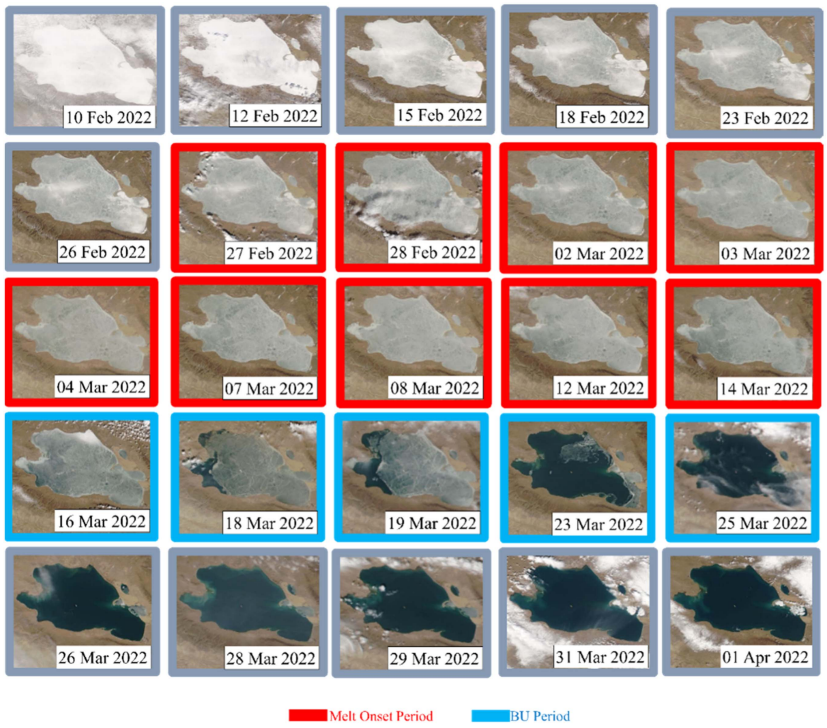

Fig. 7. MODIS images for the springtime 2022. The images with red borders refer to the melt onset period before the breakup period, which is shown with images with blue borders. This figure shows how the lake ice surface becomes darker as the overlaying snow melts.

TABLE II
MEAN BIAS ERROR (MBE) AND MEAN ABSOLUTE ERROR (MAE) FOR FUS, FUE, BUS, BUE, AND ICD BETWEEN CYGNSS AND MODIS (NUMBER OF DAYS)

	Freeze up		Break up	
	FUS	FUE	BUS	BUE
MBE	6 days	-4 days	-10 days	-4 days
MAE	7 days	5 days	10 days	4 days
ICD MBE	0 days			
ICD MAE	5 days			

by the surface roughness, and the attenuation factor owing to vegetation canopy. In the case of lake ice, only the first two are the main factors controlling the attenuation, which are the Fresnel reflection coefficient of the reflective surface and the roughness-driven decorrelation factor. Over open water, wind-generated waves can be large enough to generate a strong diffuse scattering regime, leading to the extinction of the coherent component [49]. However, as the lake transitions to the frozen state, both drivers change and, as a result, the received power varies and becomes even lower than that from open water.

B. Lake Ice Phenology Analysis Accuracy

Table II contains a summary of the average differences calculated over the four ice seasons between the CYGNSS-derived ice phenology dates and those derived from MODIS images. The MBE for FUS reveals that CYGNSS detects initial ice formation on average six days later than MODIS (MAE = 7 days). FUE, which corresponds to the date when the lake becomes fully frozen, is detected slightly earlier by CYGNSS (MBE = −4 days; MAE = 5 days). During the breakup period, BUS is determined to occur 10 days earlier (MBE = −10 days; MAE = 10 days) and BUE slightly earlier (MBE = −4 days; MAE = 4 days) from CYGNSS than the MODIS-derived dates. The MBE and MAE of ICD obtained from CYGNSS are 0 and 5 days.

C. Sensitivity of SNR Values to Spring Melt Onset

An explanation for the larger discrepancy between CYGNSS SNR and MODIS-derived timing for the beginning of the breakup period (BUS) is the sensitivity of CYGNSS SNR to spring melt onset. Spring melt onset refers to the beginning of melt of the overlying snow cover on the ice surface or of the ice surface in the absence of snow before BUS. Fig. 7 displays a set of MODIS images showing an example of the evolution of the lake ice surface during the spring of 2022, where the melt onset starts on February 27 (as determined from MODIS albedo and ERA5-Land; see Fig. 8). This process, which is associated with the temperature rise in springtime, leads to the melt of on-ice snow and causes the lake ice surface to gradually become darker before the beginning of the BUS on March 16. In Fig. 7, the images from the melt onset period are presented with red borders, whereas those from the breakup period are shown with blue borders.

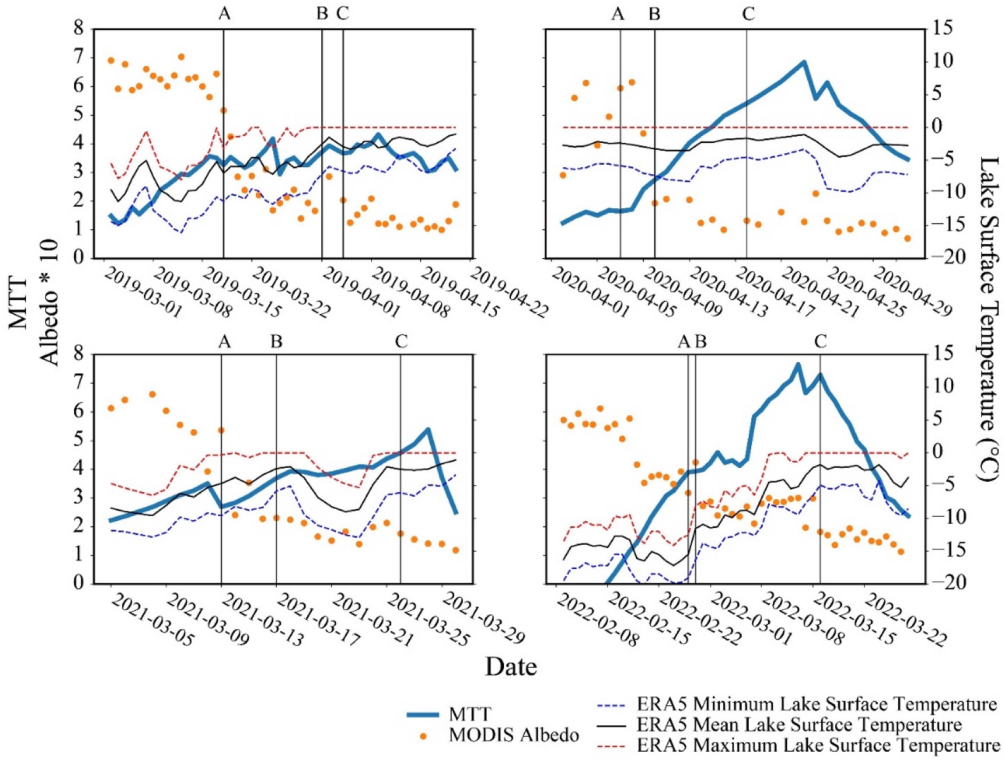

Fig. 8. Surface albedo during springtime for each year along with MTT changes. Albedo values are scaled (multiplied by 10) for display on the same axis as MTT values. Dashed lines represent the maximum, mean, and minimum lake ice surface temperatures obtained from ERA5-Land data product. Vertical black lines correspond to estimated dates of melt onset (A) from MODIS surface albedo and ERA5-Land lake ice surface temperature, CYGNSS timing for BUS (B), and MODIS-derived timing for BUS (C). The vertical black lines clearly show the sensitivity of CYGNSS to the surface melt onset.

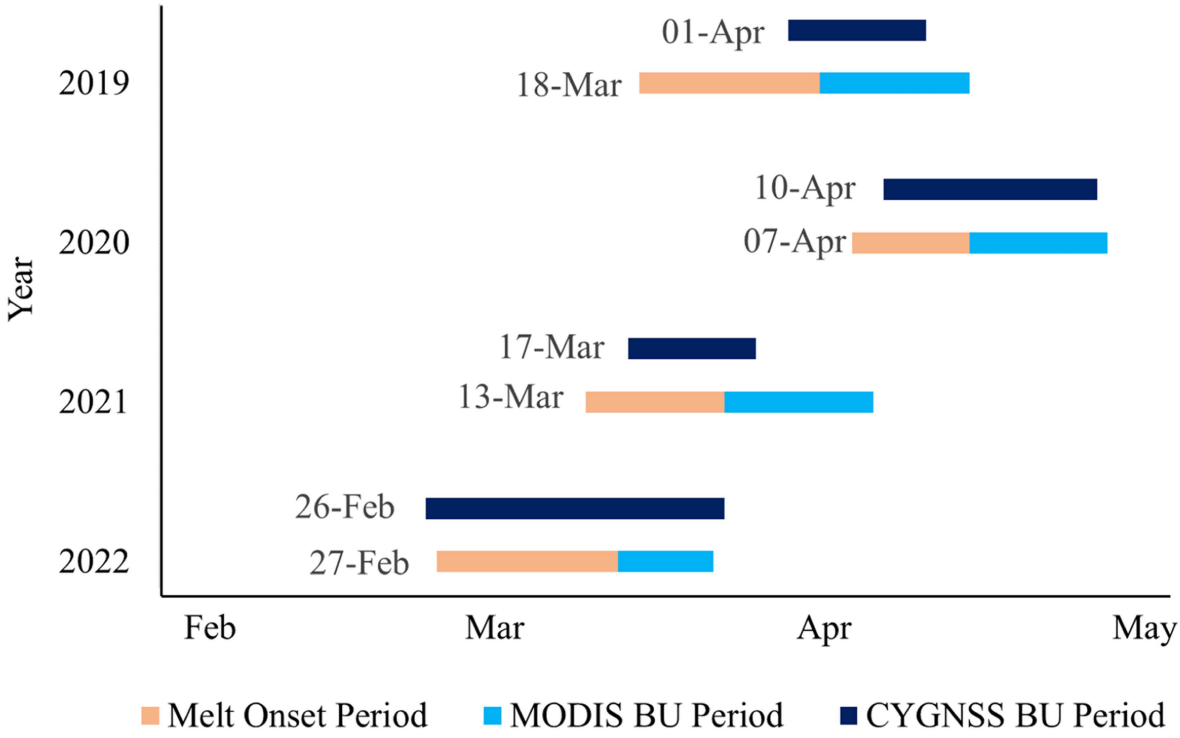

Fig. 9. CYGNSS BU period compared against the melt onset and BU periods obtained from MODIS. The BUS dates derived from CYGNSS are mostly closer to the melt onset dates rather than the BUS dates obtained from MODIS, which confirms the sensitivity of CYGNSS to the melt onset.

According to [56], spring snow melt is associated with variations in lake ice surface conditions and results in a decrease in albedo. Fig. 8 shows the changes in MODIS albedo values during the springtime for each year, in which the abrupt drops in albedo values suggest the initiation of melt onset before the BUS. These abrupt drops are associated with an increase in lake ice surface temperature. Fig. 8 also includes breakup timing obtained from CYGNSS (MTT $> t_{0.001}$) and MODIS (visually determined). Comparing spring melt onset timing with CYGNSS and MODIS breakup timing, one can see that CYGNSS timing clearly tends to be closer to the melt onset rather than BUS. This demonstrates the sensitivity of CYGNSS to the onset of spring melt before moving into the breakup period and open-water conditions.

Based on timings determined from the MODIS albedo/ERA5-Land data products, CYGNSS SNR and MODIS RGB images, which are presented together in Figs. 8 and 9, provide a time frame for the spring of each year comparing each of those timings. The time difference between the initial melt and the CYGNSS-derived breakup ranges from 1 to 13 days with MBE and MAE of 4 and 5 days, respectively, while the difference between the start of actual breakup as determined from MODIS and that of CYGNSS-derived breakup ranges from 3 to 18 days with MBE and MAE of −10 and 10 days, respectively.

D. Qinghai Lake Ice Temporal Variability

Analysis of CYGNSS SNR, which includes four freeze-up and four breakup periods, suggests that Qinghai Lake starts freezing (FUS) on either the second or the third week of December, and the freezing process lasts (FUE) until the second week of January. The FD lasts 30 days on average. On the other hand, the BUS may occur between the third week of March and the third week of April, and the BUE ranges from the last week of March to early May, suggesting that the average of BD is 13 days. These numbers are in close agreement with previous articles analyzing the temporal variability of Qinghai LIC. Using MODIS (surface reflectance) and Landsat (surface reflectance and TM/ETM+ images) products, Qi et al. [50] and [52] characterized Qinghai Lake ice phenology between 2000 and 2016 and determined the FD and BD to be, on average, 25 and 13 days, respectively. The previous articles also analyzed the spatial variability of Qinghai LIC; however, the spatial pattern of FU and BU was not examined herein since daily averages of all observations recorded from the entire lake were considered for phenology analysis.

VI. Conclusion

This article shows the ability of CYGNSS, as a space-based GNSS-Reflectometry platform, to assess the impact of lake surface (ice and open water) conditions on reflected GNSS signals and to determine the timing of lake ice phenology. Analysis of a 4-year time series of CYGNSS-derived SNR values extracted over Qinghai Lake, we observed a strong agreement between abrupt changes in SNR and the timing of freeze-up and breakup events associated with lake ice phenology visually determined from MODIS RGB images. CYGNSS measured signals were shown to be sensitive to spring surface melt prior to the first appearance of open water (BUS). The analysis supports a general finding of a previous investigation by stating that the reflected GNSS signals from LIC are significantly lower than those reflected from open water.

This investigation, however, was limited to only 4 years of observations over a single lake. To further assess the ability of GNSS-R to monitor lake ice phenology, followup studies are planned on lakes located at latitudes higher than Qinghai Lake, where GNSS-R systems can receive reflections. This will be possible with data acquired from recent and future spaceborne GNSS-R systems with polar orbits, e.g., HydroGNSS and soil moisture active passive reflectometry missions [82], [83], [84]. In addition, the analysis of data acquired along single tracks and within single footprints coincident with field measurement campaigns will further improve our understanding of the impact of lake ice conditions on reflected GNSS signals. Finally, other methods are to be explored to detect the coherency of reflections received from lakes to investigate changes in lake conditions. DDM waveform analysis using machine-learning and deep-learning techniques (e.g., [85]) is among one of the topics we are examining to detect lake ice and determine the phenology timing of Tibetan Plateau lakes and lakes located at more northern latitudes.

References

[1] C. R. Duguay, G. M. Flato, M. O. Jeffries, P. Ménard, K. Morris, and W. R. Rouse, "Ice-cover variability on shallow lakes at high latitudes: Model simulations and observations," *Hydrol. Processes*, vol. 17, no. 17, pp. 3465–3483, 2003, doi: 10.1002/hyp.1394.

[2] R. S. Williams Jr. and J. G. Ferrigno, "USGS professional paper 1386–A: State of the Earth's cryosphere at the beginning of the 21st century: Glaciers, global snow cover, floating ice, and permafrost and periglacial environments," in *USGS Professional Paper 1386–A: State of the Earth's Cryosphere at the Beginning of the 21st Century: Glaciers, Global Snow Cover, Floating Ice, and Permafrost and Periglacial Environments*. Hoboken, NJ, USA: Wiley, 2003, pp. 3465–3483, doi: 10.1002/hyp.1394.

[3] L. C. Brown and C. R. Duguay, "The response and role of ice cover in lake-climate interactions," *Prog. Phys. Geogr.: Earth Environ.*, vol. 34, no. 5, pp. 671–704, Jul. 2010, doi: 10.1177/0309133310375653.

[4] V. Mishra, K. A. Cherkauer, L. C. Bowling, and M. Huber, "Lake ice phenology of small lakes: Impacts of climate variability in the Great Lakes region," *Glob. Planet. Change*, vol. 76, no. 3/4, pp. 166–185, Apr. 2011, doi: 10.1016/j.gloplacha.2011.01.004.

[5] L. Preston et al., "Climate regulates alpine lake ice cover phenology and aquatic ecosystem structure," *Geophys. Res. Lett.*, vol. 43, no. 10, pp. 5353–5360, May 2016.

[6] L. B. Knoll et al., "Consequences of lake and river ice loss on cultural ecosystem services," *Limnology Oceanogr. Lett.*, vol. 4, no. 5, pp. 119–131, Aug. 2019, doi: 10.1002/lol2.10116.

[7] GCOS, 2022a. The 2022 GCOS Implementation Plan. WMO, GCOS-244.

[8] GCOS, 2022b. The 2022 GCOS ECVs Requirements. WMO, GCOS-245.

[9] S. Sharma et al., "Loss of ice cover, shifting phenology, and more extreme events in Northern Hemisphere Lakes," *J. Geophys. Res.: Biogeosci.*, vol. 126, no. 10, Oct. 2021, Art. no. e2021JG006348, doi: 10.1029/2021jg006348.

[10] B. Benson, "Global lake and river ice phenology database," NSIDC, 2002, doi: 10.7265/N5W66HP8.

[11] C. R. Duguay, M. Bernier, Y. Gauthier, and A. Kouraev, "Remote sensing of lake and river ice," in *Remote Sensing of the Cryosphere*. Hoboken, NJ, USA: Wiley, 2014, pp. 273–306, doi: 10.1002/9781118368909.ch12.

[12] J. Murfitt and C. R. Duguay, "50 years of lake ice research from active microwave remote sensing: Progress and prospects," *Remote Sens. Environ.*, vol. 264, Oct. 2021, Art. no. 112616, doi: 10.1016/j.rse.2021.112616.

[13] D. K. Hall and G. A. Riggs, "MODIS/aqua snow cover daily L3 global 500m grid, version 61," NASA National Snow Ice Data Center DAAC, 2021, doi: 10.5067/MODIS/MOD10A1.061.

[14] Y. Wu, C. R. Duguay, and L. Xu, "Assessment of machine learning classifiers for global lake ice cover mapping from MODIS TOA reflectance data," *Remote Sens. Environ.*, vol. 253, Feb. 2021, Art. no. 112206, doi: 10.1016/j.rse.2020.112206.
[15] Y. Cai, C. R. Duguay, and C.-Q. Ke, "A 41-year (1979–2019) passive-microwave-derived lake ice phenology data record of the Northern Hemisphere," *Earth Syst. Sci. Data*, vol. 14, no. 7, pp. 3329–3347, Jul. 2022, doi: 10.5194/essd-14-3329-2022.
[16] J. Du, J. S. Kimball, C. Duguay, Y. Kim, and J. D. Watts, "Satellite microwave assessment of Northern Hemisphere lake ice phenology from 2002 to 2015," *Cryosphere*, vol. 11, no. 1, pp. 47–63, Jan. 2017, doi: 10.5194/tc-11-47-2017.
[17] K.-K. Kang, C. R. Duguay, and S. E. L. Howell, "Estimating ice phenology on large northern lakes from AMSR-E: Algorithm development and application to Great Bear Lake and Great Slave Lake, Canada," *Cryosphere*, vol. 6, no. 2, pp. 235–254, Mar. 2012, doi: 10.5194/tc-6-235-2012.
[18] J. Murfitt and C. R. Duguay, "Assessing the performance of methods for monitoring ice phenology of the world's largest high arctic lake using high-density time series analysis of Sentinel-1 data," *Remote Sens.*, vol. 12, no. 3, Jan. 2020, Art. no. 382, doi: 10.3390/rs12030382.
[19] M. Younis, C. Fischer, and W. Wiesbeck, "Digital beamforming in SAR systems," *IEEE Trans. Geosci. Remote Sens.*, vol. 41, no. 7, pp. 1735–1739, Jul. 2003, doi: 10.1109/tgrs.2003.815662.
[20] V. U. Zavorotny, S. Gleason, E. Cardellach, and A. Camps, "Tutorial on remote sensing using GNSS bistatic radar of opportunity," *IEEE Geosci. Remote Sens. Mag.*, vol. 2, no. 4, pp. 8–45, Dec. 2014, doi: 10.1109/mgrs.2014.2374220.
[21] C. D. Hall and R. A. Cordey, "Multistatic scatterometry," in *Proc. Int. Geosci. Remote Sens. Symp., 'Remote Sens.: Moving Toward 21st Century'*, 1988, pp. 561–562, doi: 10.1109/igarss.1988.570200.
[22] M. Martín-Neira, "A passive reflectometry and interferometry system (PARIS): Application to ocean altimetry," *Ecol. Soc. Amer. J.*, vol. 17, no. 4, pp. 331–355, 1993.
[23] A. Komjathy, V. U. Zavorotny, P. Axelrad, G. H. Born, and J. L. Garrison, "GPS signal scattering from sea surface," *Remote Sens. Environ.*, vol. 73, no. 2, pp. 162–174, Aug. 2000, doi: 10.1016/s0034-4257(00)00091-2.
[24] F. Fabra et al., "Monitoring sea-ice and dry snow with GNSS reflections," in *Proc. IEEE Int. Geosci. Remote Sens. Symp.*, 2010, pp. 3837–3840, doi: 10.1109/igarss.2010.5649635.
[25] F. Fabra et al., "Phase altimetry with dual polarization GNSS-R over sea ice," *IEEE Trans. Geosci. Remote Sens.*, vol. 50, no. 6, pp. 2112–2121, Jun. 2012, doi: 10.1109/tgrs.2011.2172797.
[26] A. M. Semmling et al., "Sea-ice concentration derived from GNSS reflection measurements in fram strait," *IEEE Trans. Geosci. Remote Sens.*, vol. 57, no. 12, pp. 10350–10361, Dec. 2019, doi: 10.1109/tgrs.2019.2933911.
[27] J. F. Munoz-Martin et al., "Snow and ice thickness retrievals using GNSS-R: Preliminary results of the MOSAiC experiment," *Remote Sens.*, vol. 12, no. 24, Dec. 2020, Art. no. 4038, doi: 10.3390/rs12244038.
[28] M. D. Jacobson, "Snow-covered lake ice in GPS multipath reception—Theory and measurement," *Adv. Space Res.*, vol. 46, no. 2, pp. 221–227, Jul. 2010, doi: 10.1016/j.asr.2009.10.013.
[29] M. D. Jacobson, "A case study for inferring freshwater lake ice thickness by GPS interferometric reflectometry," *J. Geogr. Geol.*, vol. 7, no. 1, pp. 10–19, Jan. 2015, doi: 10.5539/jgg.v7n1p10.
[30] Y. Ghiasi et al., "Application of GNSS interferometric reflectometry for the estimation of lake ice thickness," *Remote Sens.*, vol. 12, no. 17, Aug. 2020, Art. no. 2721, doi: 10.3390/rs12172721.
[31] P. Jales et al., "The new Spire GNSS-R satellite missions and products," in *Proc. 26th Image Signal Process. Remote Sens.*, 2020, Art. no. 1153316, doi: 10.1117/12.2574127.
[32] V. A. Nguyen, O. Nogués-Correig, T. Yuasa, D. Masters, and V. Irisov, "Initial GNSS phase altimetry measurements from the spire satellite constellation," *Geophys. Res. Lett.*, vol. 47, no. 15, Aug. 2020, Art. no. e2020GL088308, doi: 10.1029/2020gl088308.
[33] D. Llaveria, J. F. Munoz-Martin, C. Herbert, M. Pablos, H. Park, and A. Camps, "Sea ice concentration and sea ice extent mapping with L-band microwave radiometry and GNSS-R data from the FFSCat mission using neural networks," *Remote Sens.*, vol. 13, no. 6, Mar. 2021, Art. no. 1139, doi: 10.3390/rs13061139.
[34] M. Hoseini and H. Nahavandchi, "The potential of spaceborne GNSS reflectometry for detecting ocean surface currents," *Remote Sens. Environ.*, vol. 282, Dec. 2022, Art. no. 113256, doi: 10.1016/j.rse.2022.113256.
[35] H. Carreno-Luengo et al., "The CYGNSS mission: On-going science team investigations," *Remote Sens.*, vol. 13, no. 9, 2021, Art. no. 1814, doi: 10.3390/rs13091814.
[36] M. Asgarimehr, I. Zhelavskaya, G. Foti, S. Reich, and J. Wickert, "A GNSS-R geophysical model function: Machine learning for wind speed retrievals," *IEEE Geosci. Remote Sens. Lett.*, vol. 17, no. 8, pp. 1333–1337, Aug. 2020, doi: 10.1109/lgrs.2019.2948566.
[37] C. S. Ruf et al., "A new paradigm in earth environmental monitoring with the CYGNSS small satellite constellation," *Sci. Rep.*, vol. 8, no. 1, Jun. 2018, Art. no. 8782, doi: 10.1038/s41598-018-27127-4.
[38] M. Rajabi, H. Nahavandchi, and M. Hoseini, "Evaluation of CYGNSS observations for flood detection and mapping during Sistan and Baluchestan torrential rain in 2020," *Water*, vol. 12, no. 7, Jul. 2020, Art. no. 2047, doi: 10.3390/w12072047.
[39] S. Kossieris, M. Asgarimehr, and J. Wickert, "Unsupervised machine learning for GNSS reflectometry inland water body detection," *Remote Sens.*, vol. 15, no. 12, pp. 3206–3206, 2023, doi: 10.3390/rs15123206.
[40] H. Carreno-Luengo, G. Luzi, and M. Crosetto, "Above-ground biomass retrieval over tropical forests: A novel GNSS-R approach with CYGNSS," *Remote Sens.*, vol. 12, no. 9, 2020, Art. no. 1368.
[41] M. Rahmani, J. Asgari, and M. Asgarimehr, "Soil moisture retrieval using space-borne GNSS reflectometry: A comprehensive review," *Int. J. Remote Sens.*, vol. 43, no. 14, pp. 5173–5203, 2022, doi: 10.1080/01431161.2022.2128927.
[42] M. Morris, C. Chew, J. T. Reager, R. Shah, and C. Zuffada, "A novel approach to monitoring wetland dynamics using CYGNSS: Everglades case study," *Remote Sens. Environ.*, vol. 233, 2019, Art. no. 111417, doi: 10.1016/j.rse.2019.111417.
[43] H. Carreno-Luengo, G. Luzi, and M. Crosetto, "Sensitivity of CYGNSS bistatic reflectivity and SMAP microwave radiometry brightness temperature to geophysical parameters over land surfaces," *IEEE J. Sel. Topics Appl. Earth Observ. Remote Sens.*, vol. 12, no. 1, pp. 107–122, Jan. 2019, doi: 10.1109/jstars.2018.2856588.
[44] H. Carreño-Luengo and C. S. Ruf, "Mapping freezing and thawing surface state periods with the CYGNSS based F/T seasonal threshold algorithm," *IEEE J. Sel. Topics Appl. Earth Observ. Remote Sens.*, vol. 15, pp. 9943–9952, Oct. 2022, doi: 10.1109/jstars.2022.3216463.
[45] H. Carreno-Luengo and C. S. Ruf, "Retrieving freeze/thaw surface state from CYGNSS measurements," *IEEE Trans. Geosci. Remote Sens.*, vol. 60, Oct. 2021, Art. no. 4302313, doi: 10.1109/tgrs.2021.3120932.
[46] M. Hoseini, M. Asgarimehr, H. Nahavandchi, and J. Wickert, "Spaceborne GNSS-R observations of mesoscale ocean eddies; preliminary results from CYGNSS mission," in *Proc. IEEE Int. Geosci. Remote Sens. Symp.*, 2019, pp. 8696–8699, doi: 10.1109/igarss.2019.8898461.
[47] D. Mayers and C. Ruf, "Measuring ice thickness with CYGNSS altimetry," in *Proc. IEEE Int. Geosci. Remote Sens. Symp.*, 2018, pp. 8535–8538, doi: 10.1109/igarss.2018.8519310.
[48] W. Li, E. Cardellach, F. Fabra, S. Ribó, and A. Rius, "Lake level and surface topography measured with spaceborne GNSS-reflectometry from CYGNSS mission: Example for the lake Qinghai," *Geophys. Res. Lett.*, vol. 45, no. 24, pp. 13–332, Dec. 2018, doi: 10.1029/2018gl080976.
[49] V. Zavorotny, E. Loria, A. O'Brien, B. Downs, and C. Zuffada, "Investigation of coherent and incoherent scattering from lakes using CYGNSS observations," in *Proc. IEEE Int. Geosci. Remote Sens. Symp.*, 2020, pp. 5917–5920, doi: 10.1109/igarss39084.2020.9323677.
[50] M. Qi, S. Liu, X. Yao, F. Xie, and Y. Gao, "Monitoring the Ice phenology of Qinghai Lake from 1980 to 2018 using multisource remote sensing data and Google Earth Engine," *Remote Sens.*, vol. 12, no. 14, Jul. 2020, Art. no. 2217, doi: 10.3390/rs12142217.
[51] H. Dong and Y. Song, "Shrinkage history of lake Qinghai and causes during the last 52 years," in *Proc. Int. Symp. Water Resource Environ. Protection*, 2011, pp. 446–449, doi: 10.1109/iswrep.2011.5893040.
[52] M. Qi, X. Yao, X. Li, H. Duan, Y. Gao, and J. Liu, "Spatiotemporal characteristics of Qinghai Lake ice phenology between 2000 and 2016," *J. Geogr. Sci.*, vol. 29, no. 1, pp. 115–130, Jan. 2019, doi: 10.1007/s11442-019-1587-0.
[53] C. Ruf et al., *CYGNSS Handbook*. Ann Arbor, MI, USA: Univ. Michigan Press, 2016.
[54] M. M. Al-Khaldi, J. T. Johnson, A. J. O'Brien, A. Balenzano, and F. Mattia, "Time-series retrieval of soil moisture using CYGNSS," *IEEE Trans. Geosci. Remote Sens.*, vol. 57, no. 7, pp. 4322–4331, Jul. 2019, doi: 10.1109/tgrs.2018.2890646.
[55] L. Gumley, J. Descloitres, and J. Schmaltz, *Creating Reprojected True Color MODIS Images: A Tutorial*, vol. 19. Madison, WI, USA: Univ. Wisconsin Press, 2003.

[56] S. E. L. Howell, L. C. Brown, K.-K. Kang, and C. R. Duguay, "Variability in ice phenology on Great Bear Lake and Great Slave Lake, Northwest Territories, Canada, from SeaWinds/QuikSCAT: 2000–2006," *Remote Sens. Environ.*, vol. 113, no. 4, pp. 816–834, Apr. 2009, doi: 10.1016/j.rse.2008.12.007.
[57] C. Coll, Z. Wan, and J. M. Galve, "Temperature-based and radiance-based validations of the V5 MODIS land surface temperature product," *J. Geophys. Res.*, vol. 114, Oct. 2009, Art. no. D20102, doi: 10.1029/2009jd012038.
[58] G. C. Hulley, S. J. Hook, and P. Schneider, "Optimized split-window coefficients for deriving surface temperatures from inland water bodies," *Remote Sens. Environ.*, vol. 115, no. 12, pp. 3758–3769, Dec. 2011, doi: 10.1016/j.rse.2011.09.014.
[59] K. Wang, Z. Wan, P. Wang, M. Sparrow, J. Liu, and S. Haginoya, "Evaluation and improvement of the MODIS land surface temperature/emissivity products using ground-based measurements at a semi-desert site on the western Tibetan Plateau," *Int. J. Remote Sens.*, vol. 28, no. 11, pp. 2549–2565, May 2007, doi: 10.1080/01431160600702665.
[60] G. Zhang et al., "Estimating surface temperature changes of lakes in the Tibetan Plateau using MODIS LST data," *J. Geophys. Res.: Atmos.*, vol. 119, no. 14, pp. 8552–8567, Jul. 2014, doi: 10.1002/2014jd021615.
[61] X. Zhang, K. Wang, and G. Kirillin, "An automatic method to detect lake ice phenology using MODIS daily temperature imagery," *Remote Sens.*, vol. 13, no. 14, Jul. 2021, Art. no. 2711, doi: 10.3390/rs13142711.
[62] A. G. Klein and J. Stroeve, "Development and validation of a snow albedo algorithm for the MODIS instrument," *Ann. Glaciol.*, vol. 34, pp. 45–52, 2002, doi: 10.3189/172756402781817662.
[63] C. B. Schaaf et al., "First operational BRDF, albedo nadir reflectance products from MODIS," *Remote Sens. Environ.*, vol. 83, no. 1/2, pp. 135–148, Nov. 2002, doi: 10.1016/s0034-4257(02)00091-3.
[64] Z. Wang et al., "Evaluation of moderate-resolution imaging spectroradiometer (MODIS) snow albedo product (MCD43A) over tundra," *Remote Sens. Environ.*, vol. 117, pp. 264–280, Feb. 2012, doi: 10.1016/j.rse.2011.10.002.
[65] N. A. Svacina, C. R. Duguay, and L. C. Brown, "Modelled and satellite-derived surface albedo of lake ice–Part I: Evaluation of the albedo parameterization scheme of the Canadian Lake Ice Model," *Hydrol. Processes*, vol. 28, no. 16, pp. 4550–4561, Jul. 2014, doi: 10.1002/hyp.10253.
[66] N. A. Svacina, C. R. Duguay, and J. M. L. King, "Modelled and satellite-derived surface albedo of lake ice–Part II: Evaluation of MODIS albedo products," *Hydrol. Processes*, vol. 28, no. 16, pp. 4562–4572, Jul. 2014, doi: 10.1002/hyp.10257.
[67] L. Carrea et al., "Satellite-derived multivariate world-wide lake physical variable timeseries for climate studies," *Sci. Data*, vol. 10, no. 1, Jan. 2023, Art. no. 30, doi: 10.1038/s41597-022-01889-z.
[68] L. Carrea et al., "ESA lakes climate change initiative (Lakes_cci): Lake products, version 2.0.2." NERC EDS Centre for Environmental Data Analysis, 2022, doi: 10.5285/A07DEACAFFB8453E93D57EE214676304.
[69] J. Muñoz-Sabater et al., "ERA5-land: A state-of-the-art global reanalysis dataset for land applications," *Earth Syst. Sci. Data*, vol. 13, no. 9, pp. 4349–4383, Sep. 2021, doi: 10.5194/essd-13-4349-2021.
[70] E. Loria, A. O'Brien, and I. J. Gupta, "Detection & separation of coherent reflections in GNSS-R measurements using CYGNSS data," in *Proc. IEEE Int. Geosci. Remote Sens. Symp.*, 2018, pp. 3995–3998, doi: 10.1109/igarss.2018.8517441.
[71] M. M. Al-Khaldi et al., "Inland water body mapping using CYGNSS coherence detection," *IEEE Trans. Geosci. Remote Sens.*, vol. 59, no. 9, pp. 7385–7394, Sep. 2021, doi: 10.1109/tgrs.2020.3047075.
[72] H. Carreno-Luengo, G. Luzi, and M. Crosetto, "First evaluation of topography on GNSS-R: An empirical study based on a digital elevation model," *Remote Sens.*, vol. 11, no. 21, Oct. 2019, Art. no. 2556, doi: 10.3390/rs11212556.
[73] J. Strandberg, T. Hobiger, and R. Haas, "Coastal sea ice detection using ground-based GNSS-R," *IEEE Geosci. Remote Sens. Lett.*, vol. 14, no. 9, pp. 1552–1556, Sep. 2017, doi: 10.1109/lgrs.2017.2722041.
[74] C. Chew, C. Zuffada, R. Shah, and A. Mannucci, "Mapping sea ice using reflected GNSS signals in a bistatic radar system," in *Proc. Eur. Geosci. Union Gen. Assem. Conf. Abstr.*, 2016, pp. EPSC2016–EPS10574.
[75] A. Alonso-Arroyo, V. U. Zavorotny, and A. Camps, "Sea ice detection using U.K. TDS-1 GNSS-R data," *IEEE Trans. Geosci. Remote Sens.*, vol. 55, no. 9, pp. 4989–5001, Sep. 2017, doi: 10.1109/tgrs.2017.2699122.
[76] N. Rodriguez-Alvarez, B. Holt, S. Jaruwatanadilok, E. Podest, and K. C. Cavanaugh, "An Arctic sea ice multi-step classification based on GNSS-R data from the TDS-1 mission," *Remote Sens. Environ.*, vol. 230, Sep. 2019, Art. no. 111202, doi: 10.1016/j.rse.2019.05.021.
[77] M. P. Clarizia, N. Pierdicca, F. Costantini, and N. Floury, "Analysis of CYGNSS data for soil moisture retrieval," *IEEE J. Sel. Topics Appl. Earth Observ. Remote Sens.*, vol. 12, no. 7, pp. 2227–2235, Jul. 2019, doi: 10.1109/jstars.2019.2895510.
[78] J.-M. Jiang and X.-T. You, "Where and when did an abrupt climatic change occur in China during the last 43 years?," *Theor. Appl. Climatol.*, vol. 55, no. 1–4, pp. 33–39, 1996, doi: 10.1007/bf00864701.
[79] Z. Xiao, S. Xiao, Y. Hao, and D. Zhang, "Morphological features of ionospheric response to typhoon," *J. Geophys. Res.: Space Phys.*, vol. 112, Apr. 2007, Art. no. A04304, doi: 10.1029/2006ja011671.
[80] F. T. Ulaby et al., *Microwave Radar and Radiometric Remote Sensing*. Ann Arbor, MI, USA: Univ. Michigan Press, 2014.
[81] E. Loria, A. O'Brien, V. Zavorotny, B. Downs, and C. Zuffada, "Analysis of scattering characteristics from inland bodies of water observed by CYGNSS," *Remote Sens. Environ.*, vol. 245, Aug. 2020, Art. no. 111825, doi: 10.1016/j.rse.2020.111825.
[82] N. Rodriguez-Alvarez, J. F. Muñoz-Martín, X. Bosch-Lluis, and K. Oudrhiri, "A hybrid compact polarimetry GNSS-R analysis of the Earth's Cryosphere," *IEEE Trans. Geosci. Remote Sens.*, vol. 61, May 2023, Art. no. 4301615, doi: 10.1109/tgrs.2023.3280363.
[83] D. Comite et al., "GNSS-R for sustainable development: A review of the geophysical variables addressed by the hydroGNSS mission," in *Proc. IEEE Int. Geosci. Remote Sens. Symp.*, 2022, pp. 4216–4219, doi: 10.1109/IGARSS46834.2022.9884967.
[84] M. J. Unwin et al., "An introduction to the HydroGNSS GNSS reflectometry remote sensing mission," *IEEE J. Sel. Topics Appl. Earth Observ. Remote Sens.*, vol. 14, pp. 6987–6999, Jun. 2021, doi: 10.1109/jstars.2021.3089550.
[85] M. Asgarimehr, C. Arnold, T. Weigel, C. Ruf, and J. Wickert, "GNSS reflectometry global ocean wind speed using deep learning: Development and assessment of CyGNSSnet," *Remote Sens. Environ.*, vol. 269, 2022, Art. no. 112801, doi: 10.1016/j.rse.2021.112801.

Yusof Ghiasi (Student Member, IEEE) received the B.Sc. degree in geomatics engineering from the University of Isfahan, Isfahan, Iran, in 2012, and the M.Sc. degree in geodesy from the University of Isfahan, in 2014. He is currently working toward the Ph.D. degree in GWF program with the University of Waterloo, Waterloo, ON, Canada.

He is currently a Researcher and a Data Analyst in the field of remote sensing and satellite geodesy. His academic journey took him to the University of Waterloo, where he embarked on a master's program as part of the Global Water Futures program, focusing on the innovative use of global navigation satellite system reflectometry (GNSS-R) for snow depth and lake ice thickness estimation. His research interests include space-based GNSS-R data for monitoring various aspects of lake ice physical properties, including lake ice phenology and thickness.

Claude R. Duguay (Member, IEEE) received the B.Sc. degree from the Université de Montréal, Montreal, QC, Canada, in 1983, the M.A. degree from The State University of New York at Buffalo, Buffalo, NY, USA, in 1985, and the Ph.D. degree from the University of Waterloo, Waterloo, ON, Canada, in 1989.

He is currently a Professor with the Department of Geography and Environmental Management, University of Waterloo. He is also a Founder and a Scientific Advisor of H2O Geomatics Inc., a research spin-off from the University of Waterloo. His research interests include development of physically based and machine-learning algorithms and lake products from microwave and optical satellite data, and improvement of the representation of cryospheric processes in lake model schemes implemented in numerical weather prediction and climate models. His research interests also include remote sensing, field observations, and modeling of freshwater ice with the intent of deepening our understanding and predictive capabilities of lake–atmosphere interactions in cold climate regions.

Justin Murfitt received the B.Sc. and M.Sc. degrees in geography from the University of Toronto Mississauga, Mississauga, ON, Canada, in 2012 and 2016, respectively, and the Ph.D. degree in geography from the University of Waterloo, Waterloo, ON, Canada, in 2022.

He is currently a Research Scientist working with the H2O Geomatics Inc. His research interests include using radiative transfer modeling for understanding the interaction between microwave signals and the cryosphere, as well as using machine-learning algorithms to produce operational data products for lake ice. His research interests also include the interaction between active microwave signals and lake ice at both Arctic and temperate latitudes using modeling and spaceborne platforms.

Milad Asgarimehr (Member, IEEE) received the M.Sc. degree in geodesy from the K. N. Toosi University of Technology, Tehran, Iran, in 2015.

He was awarded a Ph.D. Fellowship by Geo.X, the geoscientific competence network in Berlin and Potsdam, and joined the German Research Centre for Geosciences (GFZ) in Potsdam and Technische Universität Berlin, Berlin, Germany, in 2017. His Ph.D. dissertation was dedicated to GNSS Reflectometry and remote sensing of the ocean and atmosphere. He is currently a Researcher with the Technische Universität Berlin and GFZ. His research interests include GNSS and microwave remote sensing.

Mr. Asgarimehr was honored with the Bernd Rendel Prize in Geosciences by the German Research Foundation and successfully defended his Ph.D. in 2020 with the highest distinction.

Yuhao Wu received the B.Sc. and M.Sc. degrees in geomatics and geography from the University of Waterloo, Waterloo, ON, Canada, in 2018 and 2020, respectively.

He is currently a Data Scientist working with the H2O Geomatics Inc. His research interests include assessing remote sensing methods for monitoring ice cover and phenology on northern lakes through the development of machine-learning algorithms using satellite optical and SAR data.